

Manipulating Bell nonlocality and entanglement in polarized electron-positron annihilation

Hong-Wei Zhang,^{1, 2, *} Xu Cao,^{2, 3, 4, †} and Tai-Fu Feng^{1, ‡}

¹College of Physics Science and Technology, Hebei University, Baoding 071002, China

²Institute of Modern Physics, Chinese Academy of Sciences, Lanzhou 730000, China

³University of Chinese Academy of Sciences, Beijing 100049, China

⁴Research Center for Hadron and CSR Physics, Lanzhou University

and Institute of Modern Physics of CAS, Lanzhou 730000, China

(Dated: February 12, 2026)

The hyperon-antihyperon pairs produced in electron-positron annihilation as a massive two-qubit quantum system can be used to study the quantum correlations at high energies. This paper is theoretically dedicated to how polarization of lepton beams manipulate the Bell nonlocality and entanglement of hyperon pairs system. The response of CHSH parameter, concurrence, and negativity to the polarization degree is numerically calculated by exploiting the joint spin density matrix of $Y\bar{Y}$ system. Different influences of longitudinal and transverse polarization of beams on entanglement are found and compared. The results provide alternative perspectives for the decay of charmonium to hyperon pairs.

I. INTRODUCTION

High energy particle physics enables a new avenue of investigating entanglement and Bell non-locality, two defining characteristics of quantum mechanics which have been convincingly tested in low-energy photonic and atomic systems [1–3]. Elementary particles, e.g. top quarks [4–7] and neutrinos [8] was exploited to witness the entanglement at high energy experiment. Plenty of new proposals, for instance top-quark and τ -lepton pair at unpolarized hadron and lepton colliders [9] and polarized lepton colliders [10, 11], massless quark pair in dihadron pair production at lepton colliders [12], and electron-quark or quark-antiquark pairs at Electron-Ion Colliders [13–15], was declared as alternative environment for explore quantum entanglement.

From another landscape, maximal entanglement is conjectured as a probe of many interesting physics in hadronic field. Maximum entanglement between helicity states has been previously proposed to constrain quantum electrodynamics and weak mixing angle [16]. Maximal entanglement of partons seems to provide a new perspective in color confinement and evolution of quantum chromodynamics (QCD) [17–20] as well as hadronization [21]. Maximal entanglement would also facilitate the study of rich spin-dependent proton-proton interactions [22].

The connection between entanglement and (fundamental and approximate) symmetries of particle interactions is enlightening. Entanglement suppression in the strong interaction is found to be correlated with approximate spin-flavor symmetries, leading to emergent symmetries in low-energy baryon interactions [23]. Entangled ele-

mentary particle systems would constrain new physics beyond the Standard Model [9]. The parity-violating interactions in spin half bipartite systems is shown to disentangle the entanglement of particle pairs [24]. The influence of spin and lifetime entanglement on the decay of entangled particles is also investigated [25]. The quantum correlated $D\bar{D}$ pairs are used to measure the strong-phase differences between their decay amplitudes [26, 27].

Hyperon-antihyperon pairs produced in electron-positron annihilation can be regarded as massive qubit system [28]. Several scenarios for the observation of quantum entanglement at electron-positron colliders are suggested [29–37], leading to the recent experimental claim of the exclusion of local hidden variable theory (LHVT) after addressing several loopholes by BESIII collaboration [38]. Although experiments at colliders, in principle, do not rule out all types of hidden variable theories as discussed by several critical appraisals [39–45], the study of entanglement of elementary and composite particles is of its own interest from theoretical perspective. The non-trivial correlation of helicity states of virtual photons or charmonium produced in electron-positron annihilation results from the fact that helicity of lepton is effectively conserved in the vertex in the massless limit [46]. This is a feature of Quantum Electrodynamics (QED) related to the chiral nature of the interaction that the chiral eigenstates are the same as the helicity eigenstates for both massless particle and antiparticle spinors. Spin density matrix of hyperon and antihyperon carries forward those correlation of helicity states by virtue of the non-zero relative phase between electro and magnetic form factor in timelike region. In all previous studies, hyperon-antihyperon pairs are considered to be produced in unpolarized electron-positron collisions. This work will study how the longitudinal and transverse beam polarization manipulate the Bell nonlocality and entanglement of hyperon-antihyperon pairs.

* hweiz0929@163.com

† caoxu@impcas.ac.cn

‡ fengtf@hbu.edu.cn

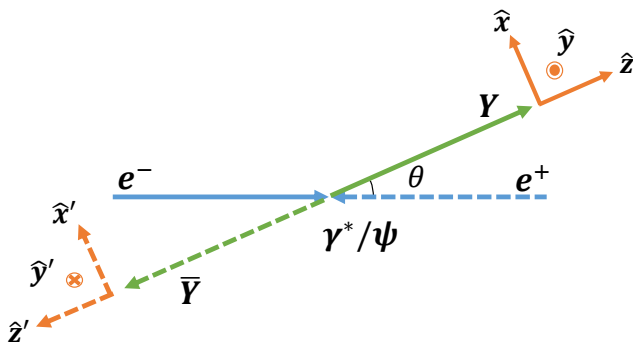


FIG. 1. The process of $e^+e^- \rightarrow \gamma^*/\psi \rightarrow Y\bar{Y}$ in the c.m. frame. The coordinate system of Y and \bar{Y} are chosen to be of the same chirality with $\{\hat{x}, \hat{y}, \hat{z}\}$ being three axes in the helicity rest frame of Y and $\{\hat{x}', \hat{y}', \hat{z}'\}$ of \bar{Y} . For hyperon Y , $\hat{y} = (\hat{\mathbf{p}}_e \times \hat{\mathbf{p}}_Y)/|\hat{\mathbf{p}}_e \times \hat{\mathbf{p}}_Y|$, $\hat{z} = \hat{\mathbf{p}}_Y$, $\hat{x} = \hat{y} \times \hat{z}$, where $\hat{\mathbf{p}}_e$ and $\hat{\mathbf{p}}_Y$ are unit vectors along momentum directions of the electron and hyperon respectively. The axes of antihyperon \bar{Y} hold the transformation: $\{\hat{x}', \hat{y}', \hat{z}'\} = \{\hat{x}, -\hat{y}, -\hat{z}\}$.

This paper is organized as follows. In Sec. II, the formalism of Bell nonlocality, concurrence, and negativity are introduced based on the spin density matrix incorporating beam polarization effects. The influence of longitudinal and transverse beam polarization is present respectively in Sec. III and Sec. IV. Hierarchy of quantum correlations and separable state are discussed in Sec. V, and the conclusion is briefly given in Sec. VI.

II. THEORETICAL SETUP

A. Spin Density Matrix

A pair of hyperon-antihyperon ($Y\bar{Y}$) both of spin half, constitutes a massive 2-qubit system, which can be fully

described by a density matrix $\rho_{Y\bar{Y}}$. As a $(1, 1)$ -type tensor on the Hilbert space $\mathcal{H} = \mathcal{H}_Y \otimes \mathcal{H}_{\bar{Y}}$, its Bloch-Fano representation reads [47]

$$\rho_{Y\bar{Y}} = \frac{1}{4} \left(I^{(4)} + \mathbf{B}^+ \cdot \boldsymbol{\sigma} \otimes I^{(2)} + I^{(2)} \otimes \mathbf{B}^- \cdot \boldsymbol{\sigma} + \sum_{i,j} C_{ij} \sigma_i \otimes \sigma_j \right), \quad i, j = 1, 2, 3, \quad (1)$$

where \mathbf{B}^\pm are polarization or Bloch vectors of hyperon and antihyperon, $\boldsymbol{\sigma}$ the vector operator combined by three Pauli matrices $\{\sigma_x, \sigma_y, \sigma_z\}$, and C_{ij} ($i, j = 1, 2, 3$) correlation tensor. Here $I^{(2)}$ and $I^{(4)}$ are 2×2 and 4×4 identity matrices, respectively. Under the basis $\{\sigma_\mu \otimes \sigma_\nu\}$ with $\sigma_0 = I^{(2)}$, the Eq. (1) also can be organized into a more compact form:

$$\rho_{Y\bar{Y}} = \frac{1}{4} \Theta_{\mu\nu} \sigma_\mu \otimes \sigma_\nu, \quad \mu, \nu = 0, 1, 2, 3, \quad (2)$$

with $\Theta_{00} = 1$, $\Theta_{i0} = B_i^+$ and $\Theta_{0j} = B_j^-$, and $\Theta_{ij} = C_{ij}$.

In $e^+e^- \rightarrow \gamma^*/\psi \rightarrow Y\bar{Y}$ process, the produced hyperon and antihyperon move in opposite directions within the center-of-mass (c.m.) frame due to momentum conservation, and the chosen coordinate system is illustrated in Fig. 1. When the electron beam is longitudinally or both electron and positron beams are transversely polarized, the non-normalized $\Theta_{\mu\nu}$ reads as [46, 48–53]

$$\Theta_{\mu\nu} = \begin{pmatrix} 1 + \alpha_\psi \cos^2 \theta & 0 & \beta_\psi \sin \theta \cos \theta & 0 \\ 0 & \sin^2 \theta & 0 & \gamma_\psi \sin \theta \cos \theta \\ -\beta_\psi \sin \theta \cos \theta & 0 & \alpha_\psi \sin^2 \theta & 0 \\ 0 & -\gamma_\psi \sin \theta \cos \theta & 0 & -\alpha_\psi - \cos^2 \theta \end{pmatrix} + P_T^2 \begin{pmatrix} \alpha_\psi \sin^2 \theta \cos 2\phi & -\beta_\psi \sin \theta \sin 2\phi & -\beta_\psi \sin \theta \cos \theta \cos 2\phi & 0 \\ -\beta_\psi \sin \theta \sin 2\phi & (\alpha_\psi + \cos^2 \theta) \cos 2\phi & -(1 + \alpha_\psi) \cos \theta \sin 2\phi & -\gamma_\psi \sin \theta \cos \theta \cos 2\phi \\ \beta_\psi \sin \theta \cos \theta \cos 2\phi & (1 + \alpha_\psi) \cos \theta \sin 2\phi & (1 + \alpha_\psi \cos^2 \theta) \cos 2\phi & -\gamma_\psi \sin \theta \sin 2\phi \\ 0 & \gamma_\psi \sin \theta \cos \theta \cos 2\phi & -\gamma_\psi \sin \theta \sin 2\phi & -\sin^2 \theta \cos 2\phi \end{pmatrix} + P_L \begin{pmatrix} 0 & \gamma_\psi \sin \theta & 0 & (1 + \alpha_\psi) \cos \theta \\ \gamma_\psi \sin \theta & 0 & 0 & 0 \\ 0 & 0 & 0 & -\beta_\psi \sin \theta \\ -(1 + \alpha_\psi) \cos \theta & 0 & -\beta_\psi \sin \theta & 0 \end{pmatrix}, \quad (3)$$

where θ is the scattering angle between the momenta of incoming electron and outgoing hyperon, e.g. $\cos \theta =$

$\hat{\mathbf{p}}_e \cdot \hat{\mathbf{p}}_Y$ in Fig. 1. The ϕ is azimuthal angle of hyperons with respect to the scattering plane. The P_T and

P_L are the transverse and longitudinal polarization degree of the beams, respectively. The $\alpha_\psi \in [-1, 1]$ is the decay parameter of the vector charmonium into hyperon and antihyperon pair, $\beta_\psi = \sqrt{1 - \alpha_\psi^2} \sin \Delta\Phi$ and $\gamma_\psi = \sqrt{1 - \alpha_\psi^2} \cos \Delta\Phi$, where $\Delta\Phi \in (-\pi, \pi]$ is the relative phase between electro- and magnetic form factor. The parameters of $J/\psi \rightarrow Y\bar{Y}$ measured by BESIII collaboration are listed in Table I.

Throughout our paper the longitudinal and transverse polarization of beams are separately considered. The Bloch vector \mathbf{B}^\pm can be read from the coefficient matrix in Eq. (3). For longitudinally polarized beam, \mathbf{B}_L^+ and \mathbf{B}_L^- are given by

$$\mathbf{B}_L^+ = \frac{1}{\chi_L} \begin{pmatrix} P_L \gamma_\psi \sin \theta \\ -\beta_\psi \sin \theta \cos \theta \\ -P_L (1 + \alpha_\psi) \cos \theta \end{pmatrix}, \quad (4)$$

$$\mathbf{B}_L^- = \frac{1}{\chi_L} \begin{pmatrix} P_L \gamma_\psi \sin \theta \\ \beta_\psi \sin \theta \cos \theta \\ P_L (1 + \alpha_\psi) \cos \theta \end{pmatrix},$$

with $\chi_L = 1 + \alpha_\psi \cos^2 \theta$, and the correlation tensor \mathbf{C}_L

is

$$\mathbf{C}_L = \frac{1}{\chi_L} \begin{pmatrix} \sin^2 \theta & 0 & \gamma_\psi \cos \theta \sin \theta \\ 0 & \alpha_\psi \sin^2 \theta & -P_L \beta_\psi \sin \theta \\ -\gamma_\psi \cos \theta \sin \theta & -P_L \beta_\psi \sin \theta & -\alpha_\psi - \cos^2 \theta \end{pmatrix}. \quad (5)$$

For transversely polarized beams, \mathbf{B}_T^+ and \mathbf{B}_T^- are

$$\mathbf{B}_T^+ = \frac{1}{\chi_T} \begin{pmatrix} -P_T^2 \beta_\psi \sin \theta \sin 2\phi \\ \beta_\psi \sin \theta \cos \theta (P_T^2 \cos 2\phi - 1) \\ 0 \end{pmatrix}, \quad (6)$$

$$\mathbf{B}_T^- = \frac{1}{\chi_T} \begin{pmatrix} -P_T^2 \beta_\psi \sin \theta \sin 2\phi, \\ \beta_\psi \sin \theta \cos \theta (1 - P_T^2 \cos 2\phi) \\ 0 \end{pmatrix},$$

with $\chi_T = 1 + \alpha_\psi \cos^2 \theta + P_T^2 \alpha_\psi \sin^2 \theta \cos 2\phi$, and the correlation tensor \mathbf{C}_T is

$$\mathbf{C}_T = \frac{1}{\chi_T} \begin{pmatrix} \sin^2 \theta + P_T^2 (\alpha_\psi + \cos^2 \theta) \cos 2\phi & -P_T^2 (1 + \alpha_\psi) \cos \theta \sin 2\phi & \gamma_\psi \sin \theta \cos \theta (1 - P_T^2 \cos 2\phi) \\ P_T^2 (1 + \alpha_\psi) \cos \theta \sin 2\phi & \alpha_\psi \sin^2 \theta + P_T^2 (1 + \alpha_\psi \cos^2 \theta) \cos 2\phi & -P_T^2 \gamma_\psi \sin \theta \sin 2\phi \\ -\gamma_\psi \sin \theta \cos \theta (1 - P_T^2 \cos 2\phi) & -P_T^2 \gamma_\psi \sin \theta \sin 2\phi & -\alpha_\psi - \cos^2 \theta - P_T^2 \sin^2 \theta \cos 2\phi \end{pmatrix}. \quad (7)$$

Notably, Eqs. (4) and (6) reveal that the hyperon possesses transverse polarization even for unpolarized beams, a distinctive feature compared to elementary particles. If the \mathbf{B}^\pm has only one non-zero component, by exchanging the axes corresponding to the non-zero transverse polarization component with the \hat{z} -axis, and afterwards rotating the coordinate system $\{\hat{\mathbf{x}}', \hat{\mathbf{y}}', \hat{\mathbf{z}}'\} = \{\hat{\mathbf{x}}, \hat{\mathbf{y}}, \hat{\mathbf{z}}\}$, and then diagonalizing the correlation matrix \mathbf{C} , the coefficient matrix $\Theta_{\mu\nu}$ always can be written into a symmetric form [34]:

$$\Theta_{\mu\nu} \rightarrow \Theta'_{\mu\nu} = \begin{pmatrix} 1 & 0 & 0 & B_z \\ 0 & \lambda_1 & 0 & 0 \\ 0 & 0 & \lambda_2 & 0 \\ B_z & 0 & 0 & \lambda_3 \end{pmatrix}, \quad (8)$$

where B_z is the non-zero polarization component of \mathbf{B}^\pm , and λ_1 , λ_2 , and λ_3 are the three eigenvalues of the correlation matrix \mathbf{C} . With the help of Eq. (2) the density matrix ρ can be expressed in the so-called X state [54]:

$$\rho \rightarrow \rho^X = \frac{1}{4} \Theta'_{\mu\nu} \sigma_\mu \otimes \sigma_\nu$$

$$= \frac{1}{4} \begin{pmatrix} 1 + 2B_z + \lambda_3 & 0 & 0 & \lambda_1 - \lambda_2 \\ 0 & 1 - \lambda_3 & \lambda_1 + \lambda_2 & 0 \\ 0 & \lambda_1 + \lambda_2 & 1 - \lambda_3 & 0 \\ \lambda_1 - \lambda_2 & 0 & 0 & 1 - 2B_z + \lambda_3 \end{pmatrix}. \quad (9)$$

The ρ and ρ^X are local unitary equivalent:

$$\rho^X = (U \otimes V) \rho (U^\dagger \otimes V^\dagger)$$

$$= \frac{1}{4} \left(I^{(4)} + B_z \sigma_z \otimes I^{(2)} + I^{(2)} \otimes B_z \sigma_z + \sum_i \lambda_i \sigma_i \otimes \sigma_i \right), \quad (10)$$

where U and V are unitary operators on Hilbert space of subsystem of ρ respectively. So that the measure of Bell nonlocality and entanglement are preserved for the transformation on ρ [55].

For hyperon-antihyperon system $\rho_{Y\bar{Y}}$, the density matrix can be reduced to a X -state in the scattering angle of $\theta = 0, \pi/2$ and π . If $\rho_{Y\bar{Y}}^{P_L}$ is the density matrix with longitudinal polarization of beam and Θ_L is its corresponding coefficient matrix, the parameters $\{B_z, \lambda_i (i = 1, 2, 3)\}$ in the symmetric form Θ'_L obtained via unitary transformation on Θ_L are given by:

$$\theta = \frac{\pi}{2} : B_z = P_L \gamma_\psi, \quad (11)$$

$$\lambda_{1,2} = \pm \sqrt{\alpha_\psi^2 + P_L^2 \beta_\psi^2}, \quad \lambda_3 = 1;$$

$$\theta = 0, \pi : B_z = -P_L, \quad \lambda_{1,2} = 0, \quad \lambda_3 = 1. \quad (12)$$

Similarly, if $\rho_{Y\bar{Y}}^{P_T}$ is the density matrix with transverse polarization of beams and Θ_T is its corresponding coefficient matrix, the parameters $\{B_z, \lambda_i (i = 1, 2, 3)\}$ in Θ'_T

matrix are

$$\theta = \frac{\pi}{2} : B_z = -\frac{P_T^2 \beta_\psi \sin 2\phi}{1 + P_T^2 \alpha_\psi \cos 2\phi},$$

$$\lambda_{1,2} = \pm \frac{\sqrt{\alpha_\psi^2 + 2P_T^2 \alpha_\psi \cos 2\phi + P_T^4 \eta}}{1 + P_T^2 \alpha_\psi \cos 2\phi},$$

$$\lambda_3 = 1; \quad (13)$$

$$\theta = 0, \pi : B_z = 0, \lambda_{1,2} = \pm P_T^2, \lambda_3 = 1. \quad (14)$$

with $\eta = \gamma_\psi^2 \sin^2 2\phi + \cos^2 2\phi$. Eq. (14) corresponds to a special case of the X-state with vanishing polarization ($\mathbf{B}^\pm = \mathbf{0}$), known as a Bell diagonal state (BDS). A local choice of basis allows such state to be expressed as a convex combination of the four maximally entangled Bell states [56],

$$\rho_{Y\bar{Y}}^{\text{BDS}} = \frac{1}{4} \left(I^{(4)} + \sum_i \lambda_i \sigma_i \otimes \sigma_i \right). \quad (15)$$

TABLE I. The parameters of $J/\psi \rightarrow Y\bar{Y}$ decay for $Y = \Lambda, \Sigma^+, \Sigma^0, \Xi^-$ and Ξ^0 measured by BESIII collaboration.

$J/\psi \rightarrow$	α_ψ	$\Delta\Phi/\text{rad}$	Ref.
$\Lambda\bar{\Lambda}$	0.475(4)	0.752(8)	[57, 58]
$\Sigma^+\bar{\Sigma}^-$	-0.508(7)	-0.270(15)	[59, 60]
$\Sigma^0\bar{\Sigma}^0$	-0.413(8)	-0.083(3)	[61]
$\Xi^-\bar{\Xi}^+$	0.586(16)	1.213(49)	[62, 63]
$\Xi^0\bar{\Xi}^0$	0.514(16)	1.168(26)	[64, 65]

B. Bell Nonlocality and Quantum Entanglement

Bell nonlocality is a fundamental quantum feature that manifests through violation of Bell-type inequalities [66, 67]. Among these, the CHSH inequality provides an experimentally viable and widely adopted framework [68]:

$$\left| \langle \hat{A}_1 \hat{B}_1 \rangle + \langle \hat{A}_1 \hat{B}_2 \rangle + \langle \hat{A}_2 \hat{B}_1 \rangle - \langle \hat{A}_2 \hat{B}_2 \rangle \right| \leq 2, \quad (16)$$

where \hat{A}_i and \hat{B}_j ($i, j = 1, 2$) denote dichotomic observables with possible outcomes $\{0, 1\}$ in two subsystems respectively. Spin operators are defined as $\hat{A}_i = \boldsymbol{\alpha}_i \cdot \boldsymbol{\sigma}$ and $\hat{B}_j = \boldsymbol{\beta}_j \cdot \boldsymbol{\sigma}$, where $\boldsymbol{\alpha}_i$ and $\boldsymbol{\beta}_j$ are unit vectors specifying measurement directions for the subsystem A and B , respectively. Then the expectation value for any bipartite state ρ is given by

$$\langle \hat{A}_i \hat{B}_j \rangle \equiv \text{Tr} [\rho (\boldsymbol{\alpha}_i \cdot \boldsymbol{\sigma} \otimes \boldsymbol{\beta}_j \cdot \boldsymbol{\sigma})]. \quad (17)$$

Since the measurement directions $\boldsymbol{\alpha}_i$ and $\boldsymbol{\beta}_j$ can be optimized to maximize the violation of CHSH inequality, the CHSH parameter $\mathcal{B}[\rho]$ is defined as the maximal violation

of the inequality with respect to the chosen measurement directions. After substituting Eq. (17) into Eq. (16), it can be expressed in closed algebraic form:

$$\begin{aligned} \mathcal{B}[\rho] &:= \max_{\boldsymbol{\alpha}_i, \boldsymbol{\beta}_j} |\boldsymbol{\alpha}_1 \cdot \mathbf{C} \cdot (\boldsymbol{\beta}_1 + \boldsymbol{\beta}_2) + \boldsymbol{\alpha}_2 \cdot \mathbf{C} \cdot (\boldsymbol{\beta}_1 - \boldsymbol{\beta}_2)| \\ &= 2\sqrt{m}. \end{aligned} \quad (18)$$

Here \mathbf{C} denotes the spin correlation matrix, and m is the sum of two largest eigenvalues of $\mathbf{C}^T \mathbf{C}$ [69], any of which ≤ 1 . For X state in Eq. (9), the eigenvalues of $\mathbf{C}^T \mathbf{C}$ read from Eq. (8) as $\{\lambda_1^2, \lambda_2^2, \lambda_3^2\}$. When $\mathcal{B}[\rho]$ lies within $(2, 2\sqrt{2}]$, the bipartite system is Bell nonlocal with $\mathcal{B} = 2\sqrt{2}$ representing the maximal Bell nonlocality.

The bipartite states can be always described by a density matrix $\rho \in \mathcal{F}_{\mathcal{H}_A \otimes \mathcal{H}_B}$, the set of all $(1, 1)$ -type tensor in a Hilbert space $\mathcal{H}_A \otimes \mathcal{H}_B$ where \mathcal{H}_A and \mathcal{H}_B are the Hilbert spaces of subsystems A and B . If the density matrix ρ can be expressed as [70]:

$$\rho = \sum_i c_i \rho_A^i \otimes \rho_B^i, \quad (19)$$

with $\sum_i c_i = 1$, $\rho_A^i \in \mathcal{F}_{\mathcal{H}_A}$ and $\rho_B^i \in \mathcal{F}_{\mathcal{H}_B}$, then the state ρ is separable and otherwise it is entangled. For a 2-qubit system, ρ is separable if and only if the partially transposed density matrix of the composite system with respect to any subsystem ρ^{T_A} or ρ^{T_B} (labeled as ρ^Γ) is positive semidefinite (Positive Partial Transpose (PPT) criterion) [71, 72]. Thus a simplified criterion is that ρ is separable if and only if [73, 74]

$$\det(\rho^\Gamma) \geq 0, \quad (20)$$

leading to the definition of the negativity as an entanglement measure [75]:

$$\mathcal{N}[\rho] = \frac{\sum_i |t_i| - 1}{2}, \quad (21)$$

where t_i are the eigenvalues of ρ^Γ . Since the partial transpose does not alter the trace of the density matrix, the presence of negative eigenvalues of ρ^Γ implies that the sum of the absolute value of the eigenvalues, $\sum_i |t_i|$, must be bigger than one. Another quantification of entanglement is Wootters' concurrence[76]:

$$\mathcal{C}[\rho] = \max \{0, k_1 - k_2 - k_3 - k_4\}, \quad (22)$$

where k_i ($i = 1, 2, 3, 4$) denote the eigenvalues (sorted in decreasing order) of the Hermitian matrix $R = \sqrt{\sqrt{\rho} \tilde{\rho} \sqrt{\rho}}$. Here $\tilde{\rho} = (\sigma_y \otimes \sigma_y) \rho^* (\sigma_y \otimes \sigma_y)$ with ρ^* being the complex conjugate of the density matrix ρ in the σ_z eigenbasis.

Both negativity and concurrence are reliable entanglement measures for 2-qubit systems given that:

- $\mathcal{C}[\rho] = 0, \mathcal{N}[\rho] = 0$ indicate a separable state;
- $\mathcal{C}[\rho] > 0, \mathcal{N}[\rho] > 0$ indicate an entangled state;

iii. $\mathcal{C}[\rho] = 1$, $\mathcal{N}[\rho] = \frac{1}{2}$ correspond to maximal entanglement.

Generally no explicit analytical relation links them. For a special case of the *rank-1* density matrix $\rho = |\psi\rangle\langle\psi|$, $\mathcal{C}(|\psi\rangle) = 2\mathcal{N}(|\psi\rangle)$ constitutes one of the necessary conditions for the system to be in a pure state. If $|P_L| = 1$ or $|P_T| = 1$, the density matrix $\rho_{Y\bar{Y}}$ in Eq. (1) reduces to a *rank-1* matrix.

Furthermore, the Peres–Horodecki criterion states that a X state in Eq. (9) is entangled if and only if either $\rho_{22}^X \rho_{33}^X < |\rho_{14}^X|^2$ or $\rho_{11}^X \rho_{44}^X < |\rho_{23}^X|^2$ holds [77] (note that two conditions cannot be simultaneously satisfied [78]). The Wootters concurrence and negativity of a X -state is given by [34, 54]

$$\begin{aligned} \mathcal{C}[\rho^X] \\ = 2 \max \left\{ 0, |\rho_{14}^X| - \sqrt{\rho_{22}^X \rho_{33}^X}, |\rho_{23}^X| - \sqrt{\rho_{11}^X \rho_{44}^X} \right\}, \end{aligned} \quad (23)$$

$$\begin{aligned} \mathcal{N}[\rho^X] \\ = -\min \left\{ 0, \frac{\rho_{11}^X + \rho_{44}^X}{2} - \sqrt{\left(\frac{\rho_{11}^X - \rho_{44}^X}{2} \right)^2 + \rho_{23}^X}, \right. \\ \left. \frac{\rho_{22}^X + \rho_{33}^X}{2} - \sqrt{\left(\frac{\rho_{22}^X - \rho_{33}^X}{2} \right)^2 + \rho_{14}^X} \right\}. \end{aligned} \quad (24)$$

resulting into $\mathcal{C}[\rho_{Y\bar{Y}}^X] = 2\mathcal{N}[\rho_{Y\bar{Y}}^X] = |\lambda_2|$ at $\theta = 0, \pi/2$ and π .

III. LONGITUDINAL BEAM POLARIZATION

The section will discuss the impact of longitudinal polarization of beams on Bell-nonlocality and quantum entanglement. Only the results of $J/\psi \rightarrow Y\bar{Y}$ decay for $Y = \Lambda, \Sigma^+, \Xi^-,$ and Ξ^0 are shown, see Appendix A for $J/\psi \rightarrow \Sigma^0\bar{\Sigma}^0$ and $\psi(3686) \rightarrow Y\bar{Y}$. However, the conclusions for $J/\psi \rightarrow \Sigma^0\bar{\Sigma}^0$ will also be presented in the main text, and any conclusions that do not hold universally across all channels are explicitly noted.

The θ and P_L dependence of the CHSH parameter $\mathcal{B}[\rho_{Y\bar{Y}}^{P_L}]$ are shown in Fig. 2 with the parameters in Table I. Note that $\mathcal{B}(\theta) = \mathcal{B}(\pi - \theta)$ with $\theta \in [0, \pi]$, and $\mathcal{B}(P_L) = \mathcal{B}(-P_L)$ with $P_L \in [-1, 1]$. It can be seen that increasing P_L enhances Bell-nonlocality across the full range of θ with an exception of $\theta = 0$ and π , under which angles $\mathcal{B} \equiv 2$ is independent on P_L (see Eq. (12)). In Fig. 2, the area between two dashed lines in each panel represents Bell-nonlocally $\mathcal{B} \in (2, \max_\theta \mathcal{B}]$ with $\max_\theta \mathcal{B}$ being the largest CHSH parameter. The $\max_\theta \mathcal{B}$ is present at $\theta = \pi/2$ at any P_L for all channels, see Eq. (11):

$$\max \mathcal{B} = \mathcal{B}(\theta = \frac{\pi}{2}) = 2\sqrt{1 + \alpha_\psi^2 + P_L^2 \beta_\psi^2} < 2\sqrt{2} \quad (25)$$

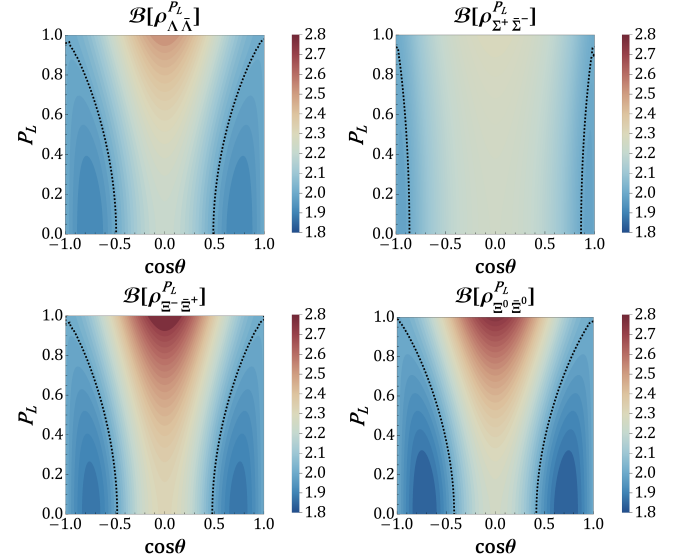


FIG. 2. The CHSH parameter $\mathcal{B}[\rho_{Y\bar{Y}}^{P_L}]$ as a function of $\cos\theta$ (θ is the scattering angle) and longitudinal beam polarization degree P_L in $J/\psi \rightarrow Y\bar{Y}$ for $Y = \Lambda, \Sigma^+, \Xi^-,$ and Ξ^0 . The dashed curve is for $\mathcal{B}[\rho_{Y\bar{Y}}^{P_L}] = 2$.

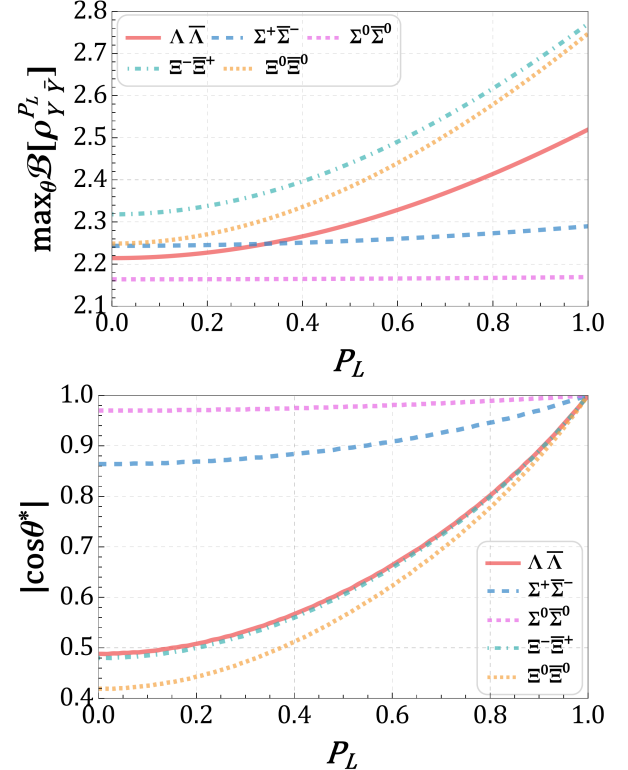


FIG. 3. The $\max_\theta \mathcal{B}[\rho_{Y\bar{Y}}^{P_L}]$ (upper panel) and $\cos\theta^*$ (lower panel, see main text for definition of θ^*) as a function of P_L in $J/\psi \rightarrow Y\bar{Y}$ for $Y = \Lambda, \Sigma^+, \Xi^-$ and Ξ^0 .

which is displayed in the upper panel of Fig. 3.

Increasing P_L expands the angular coverage of Bell nonlocality as can be also seen in Fig. 2. The correspond-

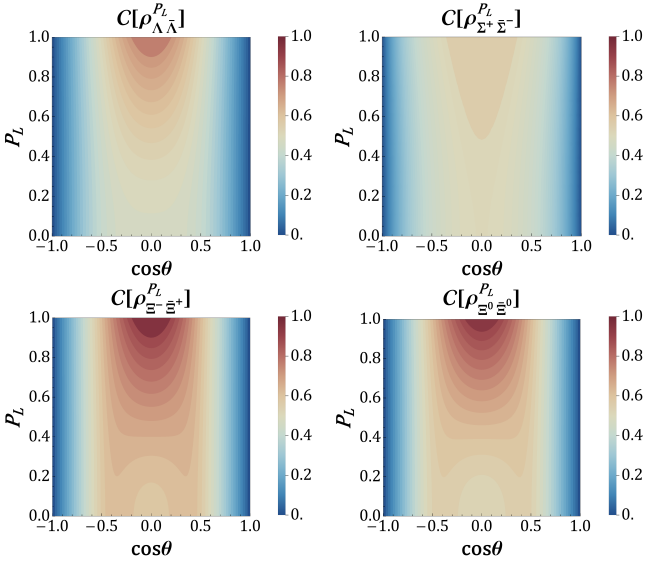


FIG. 4. The concurrence $C[\rho_{Y\bar{Y}}^{P_L}]$ as a function of $\cos\theta$ and P_L in $J/\psi \rightarrow Y\bar{Y}$ for $Y = \Lambda, \Sigma^+, \Xi^-$ and Ξ^0 .

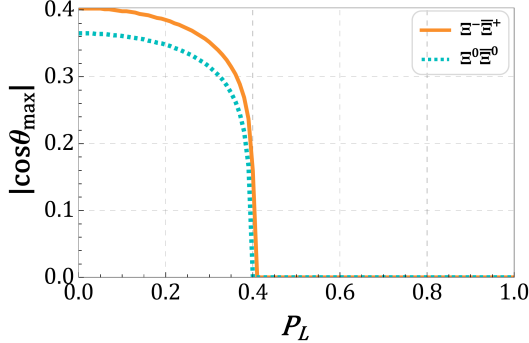


FIG. 5. The $\cos\theta_{\max}$ (see main text for definition of θ_{\max}) as a function of P_L in $J/\psi \rightarrow Y\bar{Y}$ for $Y = \Xi^-$ and Ξ^0 .

ing angle for $\mathcal{B}[\rho_{Y\bar{Y}}^{P_L}] = 2$ is defined as the critical angle θ^* , shown in the lower panel of Fig. 3. The $|\cos\theta^*|$ moves to 1 when P_L is approaching the maximum degree, so that the system of hyperon pairs is always Bell-nonlocal across the range $\theta \in (0, \pi)$ at $P_L = 1$. It is noted that for Σ^+ and Σ^0 channels \mathcal{B} exhibits relatively low dependence on P_L , and θ^* is already close to zero in the case of unpolarized beams.

Fig. 4 shows that the θ and P_L dependence of the concurrence $C[\rho_{Y\bar{Y}}^{P_L}]$. The negativity $\mathcal{N}[\rho_{Y\bar{Y}}^{P_L}]$ is shown by Fig. 15 in Appendix A. It can be seen that a higher degree of longitudinal polarization leads to enhanced concurrence C and negativity \mathcal{N} over the full θ range with a exception of $\theta = 0$ and π , from Eqs. (12), (23) and (24), under which angles $C = 2\mathcal{N} \equiv 0$ means that the states are separable and is independent on P_L .

The largest negativity with respect to θ , labeled as $\max_\theta \mathcal{N}$, locates at $\theta = \pi/2$ across the full P_L range for all channels. The position of the largest concurrence with respect to θ , denoted as $\max_\theta C$, lies:

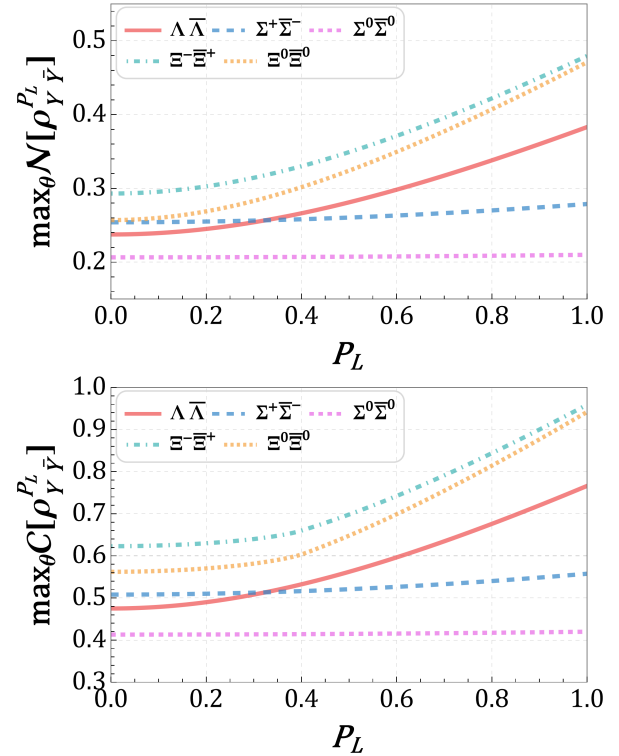


FIG. 6. The $\max_\theta \mathcal{N}[\rho_{Y\bar{Y}}^{P_L}]$ (upper panel) and $\max_\theta C[\rho_{Y\bar{Y}}^{P_L}]$ (lower panel) as a function of P_L in $J/\psi \rightarrow Y\bar{Y}$ for $Y = \Lambda, \Sigma^+, \Sigma^0, \Xi^-$ and Ξ^0 .

- at $\theta = \pi/2$ across the full P_L range for Λ, Σ^+ and Σ^0 channels;
- at the angles of $\theta = \theta_{\max}$ and $\pi - \theta_{\max}$ when P_L is small, and moves to $\theta = \pi/2$ as the P_L is increasing to certain value for Ξ^- and Ξ^0 channels.

For the later case the $|\cos\theta_{\max}|$ is plotted as a function of P_L in Fig. 5. It can be found that at $P_L \gtrsim 0.4$ the $\max_\theta \mathcal{C}$ is shifted to $\theta = \pi/2$ for both channels. From Eqs. (11), (23) and (24), one has

$$\mathcal{C}(\theta = \frac{\pi}{2}) = 2\mathcal{N}(\theta = \frac{\pi}{2}) = \sqrt{\alpha_\psi^2 + P_L^2\beta_\psi^2}, \quad (26)$$

As shown in Fig. 6, $\max_\theta \mathcal{N}$ and $\max_\theta \mathcal{C}$ increases monotonically as the increase of P_L for all channels. They both reach the largest extrema at $P_L = 1$, but not maximal entangled since $\max_\theta \mathcal{C} < 1$ persists. The $\max_\theta \mathcal{N}$ and $\max_\theta \mathcal{C}$ (likewise $\max_\theta \mathcal{B}$) of Σ^+ and Σ^0 channels are insensitive to P_L .

IV. TRANSVERSE BEAM POLARIZATION

The situation for transverse polarization is more complicated considering that it introduces the dependence on the azimuthal angle ϕ with respect to the scattering plane. Fig. 7 displays the P_T and ϕ dependence

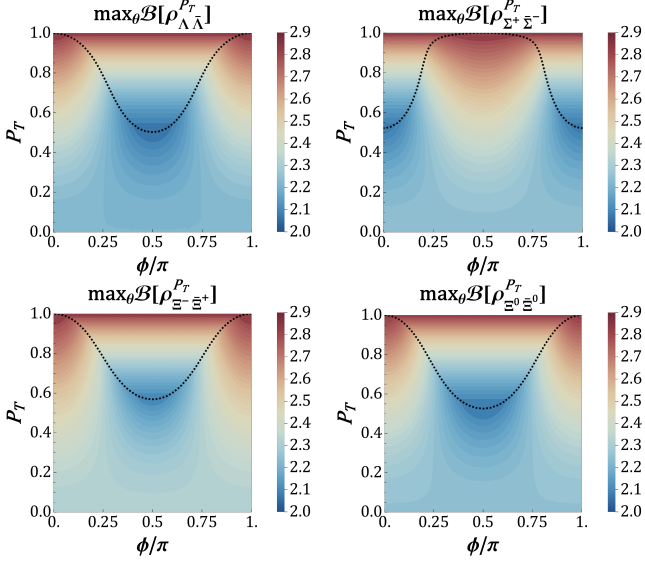


FIG. 7. The $\max_{\theta} B[\rho_{Y\bar{Y}}^{P_T}]$ as a function of azimuthal angle ϕ and transverse beams polarization degree P_T in $J/\psi \rightarrow Y\bar{Y}$ for $Y = \Lambda$, Σ^+ , Ξ^- and Ξ^0 . The dashed curve is for $B(\theta = 0, \pi) = B(\theta = \pi/2)$.

of the largest CHSH parameter with respect to θ , labeled as $\max_{\theta} B[\rho_{Y\bar{Y}}^{P_T}]$, with a note of $B(\theta) = B(\pi - \theta)$ with $\theta \in [0, \pi]$, $B(P_T) = B(-P_T)$ with $P_T \in [-1, 1]$ and $B(\phi) = B(\pi - \phi)$, $B(\phi) = B(\pi + \phi)$ with $\phi \in [0, \pi]$. The $\max_{\theta} B$ happens either at $\theta = 0, \pi$ or $\theta = \pi/2$, which can be derived from Eq. (13),

$$B(\theta = 0, \pi) = 2\sqrt{1 + P_T^4}, \quad (27)$$

$$B(\theta = \frac{\pi}{2}) = \frac{2\sqrt{1 + \alpha_{\psi}^2 + 4P_T^2\alpha_{\psi}\cos 2\phi + P_T^4\varepsilon}}{1 + P_T^2\alpha_{\psi}\cos 2\phi}, \quad (28)$$

with $\varepsilon = \beta_{\psi}^2 \cos^2 2\phi + \gamma_{\psi}^2$. The dashed curve $B(\theta = 0, \pi) = B(\theta = \pi/2)$ in Fig. 7 divides each panel into two regions. For the region above the dashed curve, the $\max_{\theta} B$ occurs at $\theta = 0, \pi$, and attain maximal violation of CHSH inequality for arbitrary ϕ at $P_T = 1$ from Eq. (27). For the region below the dashed curve, the $\max_{\theta} B$ occurs at $\theta = \pi/2$, and hold the maximal violation for $\phi = 0$ and π at $P_T = 1$ from Eq. (28). It is found for both regions $\max_{\theta} B \geq 2$ across full ϕ coverage, and $P_T = 1$ drives $\max_{\theta} B$ to approach $2\sqrt{2}$ at any fixed ϕ .

As can be seen in Fig. 7, the largest value of $\max_{\theta} B[\rho_{Y\bar{Y}}^{P_T}]$, here labeled as $\max_{\theta, \phi} B[\rho_{Y\bar{Y}}^{P_T}]$, is attained at specific angles ϕ with P_T held constant. As shown in upper panel of Fig. 8, the $\max_{\theta, \phi} B$ is always enhanced as the increase of P_T , and occurs at specific angles of

- a. $\phi = k\pi$ ($k = 0, 1, 2$) for Λ , Ξ^- and Ξ^0 channels;
- b. $\phi = \pi/2 + k\pi$ ($k = 0, 1$) for Σ^+ , Σ^0 channels.

The violation of CHSH inequality across full θ range can be achieved by increasing the transverse beams polarization degree P_T . Therefore a minimal P_T required

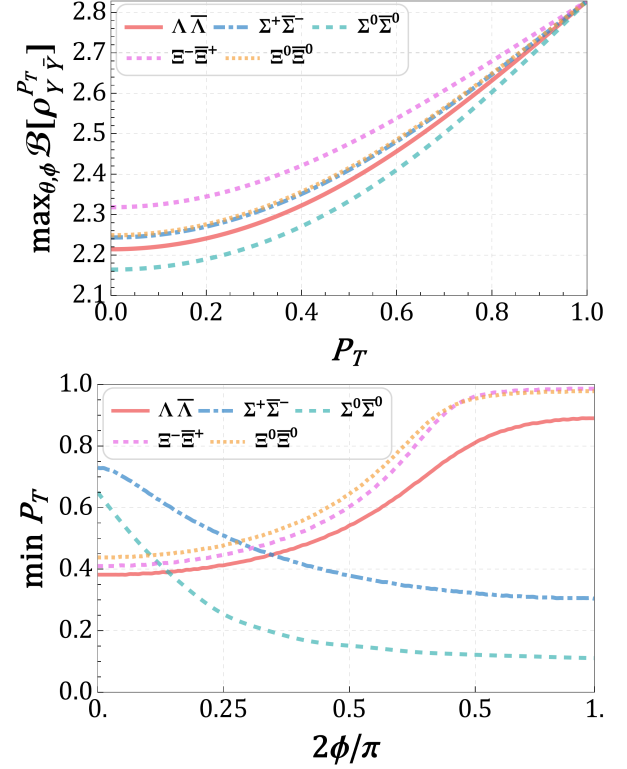


FIG. 8. The $\max_{\theta, \phi} B[\rho_{Y\bar{Y}}^{P_T}]$ as a function of P_T (upper panel), and the minimal transverse polarization $\min P_T(\phi)$ required to achieve $B[\rho_{Y\bar{Y}}^{P_T}] = 2$ as a function of ϕ (lower panel) for all five channels.

to achieve $B[\rho_{Y\bar{Y}}^{P_L}] \geq 2$ across full θ range, labeled as $\min P_T$, can be defined as a function of ϕ , as shown in lower panel of Fig. 8. The $\min P_T$ increases as the increase of $\phi \in [0, \pi/2]$ for Λ , Ξ^- and Ξ^0 channels, opposite to the trends of Σ^+ and Σ^0 channels.

The largest concurrence and negativity with respect to θ , labeled as $\max_{\theta} \mathcal{C}[\rho_{Y\bar{Y}}^{P_T}]$ and $\max_{\theta} \mathcal{N}[\rho_{Y\bar{Y}}^{P_T}]$, respectively, can be similarly defined. The behaviour of $\max_{\theta} \mathcal{C}$ in Fig. 9 and $\max_{\theta} \mathcal{N}$ in Appendix. A as a function of P_T and ϕ are similar to $\max_{\theta} B$. The position of $\max_{\theta} \mathcal{C}$ lies:

- a. Λ , Σ^- and Σ^0 channels: either at $\theta = 0, \pi$ for the region above the dashed curve, or at $\theta = \pi/2$ for the region below the dashed curve.
- b. Ξ^- and Ξ^0 channels: either at $\theta = 0, \pi$ for the region above the dashed curve, or $\cos \theta = 0.365$ (for Ξ^-) and 0.403 (for Ξ^0) for the region below the dashed curve.

For the position of $\max_{\theta} \mathcal{N}$, case-a is applied for all channels. From Eqs. (13), (14), (23) and (24), one read as

$$\mathcal{C}(\theta = 0, \pi) = 2\mathcal{N}(\theta = 0, \pi) = P_T^2, \quad (29)$$

$$\mathcal{C}(\theta = \frac{\pi}{2}) = 2\mathcal{N}(\theta = \frac{\pi}{2}) = \frac{\sqrt{\alpha_{\psi}^2 + 2P_T^2\alpha_{\psi}\cos 2\phi + P_T^4\eta}}{1 + P_T^2\alpha_{\psi}\cos 2\phi}, \quad (30)$$

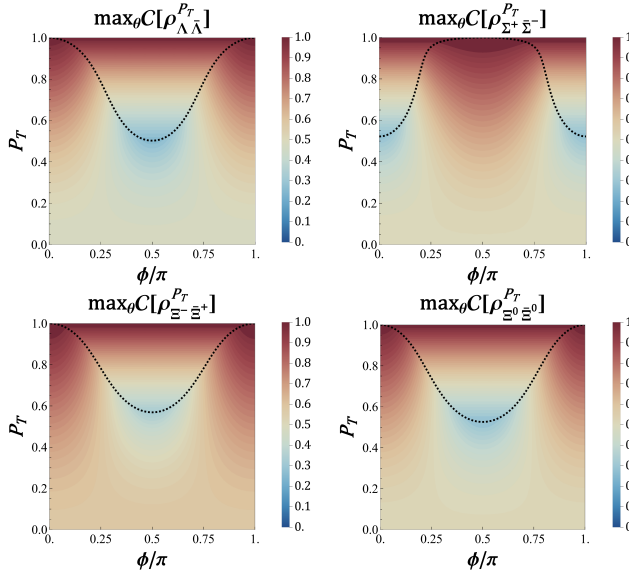


FIG. 9. The $\max_{\theta} \mathcal{C}[\rho_T]$ as a function of ϕ and P_T in $J/\psi \rightarrow Y\bar{Y}$ for $Y = \Lambda, \Sigma^+, \Xi^-$ and Ξ^0 . See main text for a detailed explanation of the dashed lines.

From Eq. (29), maximal entanglement is attained at $\theta = 0$ and π for arbitrary ϕ if $P_T = 1$. From Eq. (30), maximal entanglement is attained at $\theta = \pi/2$ for $\phi = 0$ and π if $P_T = 1$.

Similar to $\max_{\theta,\phi} \mathcal{B}$, $\max_{\theta,\phi} \mathcal{C}$ and $\max_{\theta,\phi} \mathcal{N}$ can be defined as the largest value of $\max_{\theta} \mathcal{C}$ and $\max_{\theta} \mathcal{N}$ at specific angles ϕ with P_T held constant, respectively. The $\max_{\theta,\phi} \mathcal{C}$ and $\max_{\theta,\phi} \mathcal{N}$, locating at the same azimuthal angle ϕ as that of $\max_{\theta,\phi} \mathcal{B}$, increase monotonically as the increase of P_T as shown in Fig. 10. For $P_T = 1$, the system can always attain maximal entanglement under the proper selection of ϕ and θ angles, as also can be seen in Fig. 9 that $\max_{\theta} \mathcal{C} = 2 \max_{\theta} \mathcal{N} = 1$ at any fixed ϕ at $P_T = 1$.

V. DISCUSSIONS

In this section hierarchy of quantum correlations and separable state will be discussed in detail.

A. Hierarchy of Quantum Correlations

Bell nonlocality and quantum entanglement satisfy following hierarchy with respect to quantumness:

$$\text{Bell nonlocality} \subset \text{Quantum entanglement}.$$

The CHSH parameter $\mathcal{B}[\rho]$ of bipartite system is constrained with regard to the Wootters' concurrence $\mathcal{C}[\rho]$ [79]:

$$\mathcal{B}[\rho] \leq 2 \sqrt{1 + \mathcal{C}^2[\rho]}. \quad (31)$$

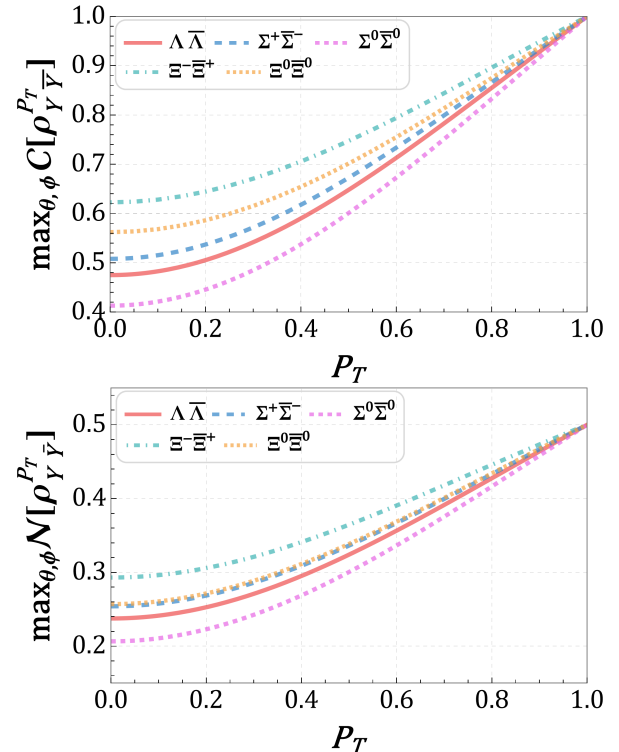


FIG. 10. The $\max_{\theta,\phi} \mathcal{C}[\rho_{Y\bar{Y}}^P]$ (upper) and $\max_{\theta,\phi} \mathcal{N}[\rho_{Y\bar{Y}}^P]$ (lower) as a function of P_T in $J/\psi \rightarrow Y\bar{Y}$ for $Y = \Lambda, \Sigma^+, \Sigma^0, \Xi^-$ and Ξ^0 respectively.

A sufficient but unnecessary condition for the equality hold (except for pure state) is that the two-qubit system is BDS [79]. On the other hand, an upper bound of Wootters' concurrence is given in terms of the polarization of subsystems[80]:

$$\mathcal{C}[\rho] \leq \min \left\{ \sqrt{1 - |\mathbf{B}^+|^2}, \sqrt{1 - |\mathbf{B}^-|^2} \right\}, \quad (32)$$

Thus the possible largest entanglement between the each subsystems of 2-qubit decreases as the polarization degree increases. By combining Eq. (31) and Eq. (32), an bound for the CHSH parameter is derived:

$$\mathcal{B}[\rho] \leq \min \left\{ 2 \sqrt{2 - |\mathbf{B}^+|^2}, 2 \sqrt{2 - |\mathbf{B}^-|^2} \right\}. \quad (33)$$

The above inequality becoming an equality if and only if Eqs. (31) and (32) are both saturated. As a special case in which the entanglement is always maximal, Eq. (33) is trivially saturated for the elementary particle of $\mathbf{B}^{\pm} = 0$ [10, 11].

For hyperon-antihyperon pairs, Eq. (31) becomes an equality at $\theta = 0, \pi/2$, and π regardless of the polarization of beams as shown in Sec. III and IV. Furthermore, from Eqs. (4) and (6) the $|\mathbf{B}^+| = |\mathbf{B}^-|$ always holds,

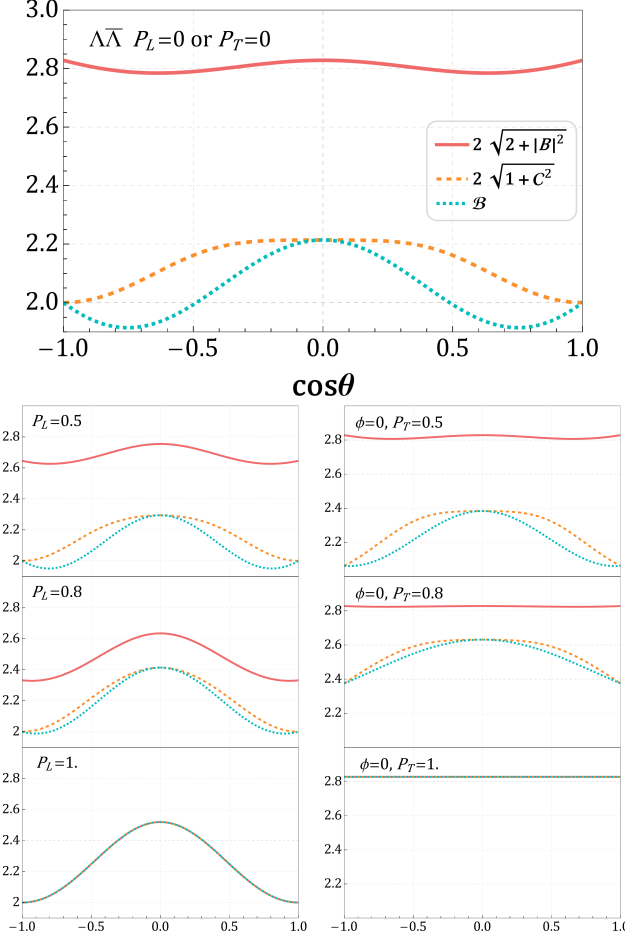


FIG. 11. Upper bounds in Eq. (31) (orange dashed lines) and Eq. (33) (red solid lines) for Λ channel are compared to the CHSH parameters $\mathcal{B}[\rho]$ (green dotted lines) as a function of $\cos\theta$. Upper panel: unpolarized lepton beams. Lower left panels: longitudinal polarized electron beam. Lower right panels: transversely polarized lepton beams with $\phi = 0$. The polarization degrees P_L or P_T are indicated in each panel.

resulting into:

$$|\mathbf{B}_L| = \frac{1}{\chi_L} \sqrt{\beta_\psi^2 \sin^2 \theta \cos^2 \theta + P_L^2 (\beta_\psi^2 \cos^2 \theta + \gamma_\psi^2)}, \quad (34)$$

$$|\mathbf{B}_T| = \frac{\beta_\psi \sin \theta}{\chi_T} \sqrt{(1 - P_T^2 \cos 2\phi)^2 \cos^2 \theta + P_T^4 \sin^2 2\phi}. \quad (35)$$

A necessary condition for the existence of maximal entanglement ($\mathcal{C} = 1$) is that the system is in a pure state. When $P_L = 1$ or $P_T = 1$, the $\rho_{Y\bar{Y}}$ is in a pure state and the Eq. (33) hold as equality. As can be seen, polarization of hyperons is non-vanishing ($\mathbf{B}_L^\pm \neq \mathbf{0}$) across full scattering angular coverage on the condition of maximizing longitudinal beam polarization degree. Therefore maximal entanglement is never unachievable since $\mathcal{C}[\rho_{Y\bar{Y}}^{P_L}] < 1$ as constrained by Eq. (32). Even so, the system accesses

the largest possible entanglement. On the other hand, tuning the transverse polarization degree to maximum degree makes it possible to realize vanishing polarization of hyperons by properly choosing θ and ϕ as shown by Eq. (35) and discussed in Sec. IV.

Taking Λ channel as an example, Fig. 11 shows the evolution of the upper bounds in Eqs. (31) and (33) as the longitudinal or transverse beam polarization degree increases in comparison of the CHSH parameters $\mathcal{B}[\rho_{\Lambda\bar{\Lambda}}]$. The upper bounds in Eq. (31) is more stringent than that in Eq. (33). When the P_L or P_T approaches the maximum degree, and two upper bounds become close to each other and ultimate equal at any scattering angle when the system is in a pure state. It can be also seen in Fig. 11 that if $P_T = 1$, maximal entanglement is attained across full θ range at particular angles $\phi = k\pi, (k = 0, 1, 2)$.

B. Separable state with transversely polarized beams

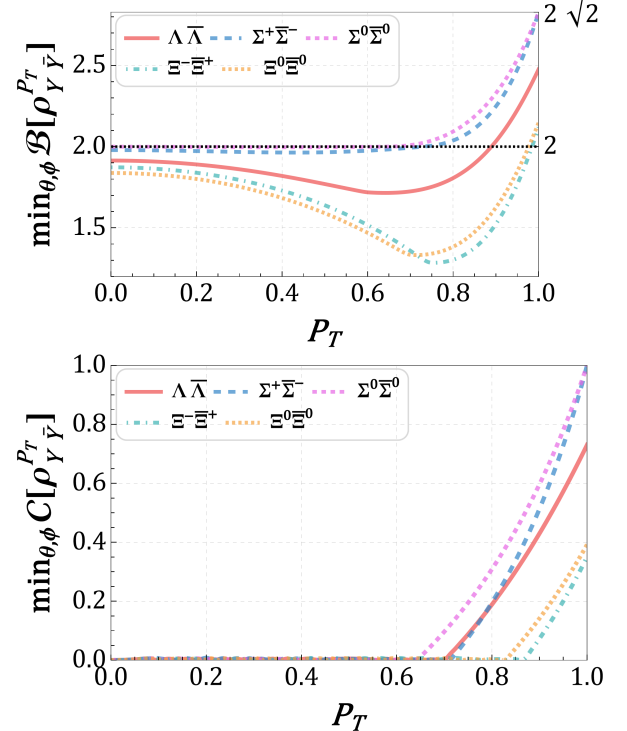


FIG. 12. The $\min_{\theta, \phi} \mathcal{B}[\rho_{Y\bar{Y}}^{P_T}]$ (upper) and $\min_{\theta, \phi} \mathcal{C}[\rho_{Y\bar{Y}}^{P_T}]$ (lower) as a function of P_T in $J/\psi \rightarrow Y\bar{Y}$ for $Y = \Lambda, \Sigma^+, \Sigma^0, \Xi^-$ and Ξ^0 respectively.

In the case of transverse polarized beams, minimum values of $\mathcal{B}[\rho_{Y\bar{Y}}^{P_T}]$ and $\mathcal{C}[\rho_{Y\bar{Y}}^{P_T}]$, labeled as $\min_{\theta, \phi} \mathcal{B}[\rho_{Y\bar{Y}}^{P_T}]$ and $\min_{\theta, \phi} \mathcal{C}[\rho_{Y\bar{Y}}^{P_T}]$, can be found across the full range of solid angle, as shown in Fig. 12. It is observed that over a substantial P_T range the system is of vanishing entanglement, and the CHSH inequality is not violated, indicating

the separability of the system at certain azimuthal angle ϕ^* :

- a. $\phi^* = k\pi, (k = 0, 1, 2)$ for Σ^+ , Σ^0 channels with $\alpha_\psi < 0$;
- b. $\phi^* = \pi/2 + k\pi, (k = 0, 1)$ for Λ , Ξ^- , and Ξ^0 channels with $\alpha_\psi > 0$.

At these ϕ^* , \mathbf{B}_T^\pm in Eq. (6) has only one nonzero component, and the $\rho_{Y\bar{Y}}^{P_T}$ as a X -state with the parameters in Eq. (8) are given by

$$\begin{aligned} B_z &= -\frac{\beta_\psi (1 \mp P_T^2) \sin 2\theta}{2\chi'_T}, \\ \lambda_1 &= \frac{(1 \pm P_T^2)(1 + \alpha_\psi) + (1 \mp P_T^2)\sqrt{\zeta}}{2\chi'_T}, \\ \lambda_2 &= \frac{(1 \pm P_T^2)(1 + \alpha_\psi) - (1 \mp P_T^2)\sqrt{\zeta}}{2\chi'_T}, \\ \lambda_3 &= -\frac{\alpha_\psi \sin^2 \theta \pm P_T^2 (1 + \alpha_\psi \cos^2 \theta)}{\chi'_T}. \end{aligned} \quad (36)$$

with $\chi'_T = 1 + \alpha_\psi \cos^2 \theta \pm P_T^2 \alpha_\psi \sin^2 \theta$ and $\zeta = (\alpha_\psi + \cos 2\theta)^2 + \gamma_\psi^2 \sin^2 2\theta$. The upper and lower sign of “ \pm ” and “ \mp ” are for case-a and case-b of ϕ^* , respectively. From Eqs. (23) and (24), $\min_\phi \mathcal{B}[\rho_{Y\bar{Y}}^{P_T}]$, $\min_\phi \mathcal{C}[\rho_{Y\bar{Y}}^{P_T}]$ and $\min_\phi \mathcal{N}[\rho_{Y\bar{Y}}^{P_T}]$ are given by:

$$\min_\phi \mathcal{B}[\rho_{Y\bar{Y}}^{P_T}] = 2\sqrt{m'}, \quad (37)$$

$$\min_\phi \mathcal{C}[\rho_{Y\bar{Y}}^{P_T}] = 2 \min_\phi \mathcal{N}[\rho_{Y\bar{Y}}^{P_T}] = |\lambda_2|. \quad (38)$$

where m' is the sum of two largest eigenvalues of $\{\lambda_1^2, \lambda_2^2, \lambda_3^2\}$ in Eq. (36).

For each channel, when the polarization degree P_T is increased to be a critical value, nonseparability of the system is emergent. If P_T keeps increasing to another critical value, the Bell nonlocality of the system appears with the CHSH inequality violated. This is consistent with the hierarchy of quantum correlations mentioned in Sec. V A. Those critical values are summarized in Table. II.

TABLE II. The critical P_T values of $J/\psi \rightarrow Y\bar{Y}$ for $Y = \Lambda$, Σ^+ , Σ^0 , Ξ^- and Ξ^0 .

$J/\psi \rightarrow$	Bell nonlocality	Nonseparability
$\Lambda\bar{\Lambda}$	0.890	0.695
$\Sigma^+\bar{\Sigma}^-$	0.761	0.679
$\Sigma^0\bar{\Sigma}^0$	0.681	0.609
$\Xi^-\bar{\Xi}^+$	0.987	0.865
$\Xi^0\bar{\Xi}^0$	0.971	0.820

The system is separable with fixed P_T and ϕ^* at scattering angles θ_{Sep} and $\pi - \theta_{Sep}$, indicating from Eq. (38) that

$$\min_\phi \mathcal{C}(\theta_{Sep}) = 2 \min_\phi \mathcal{N}(\theta_{Sep}) = |\lambda_2| = 0. \quad (39)$$

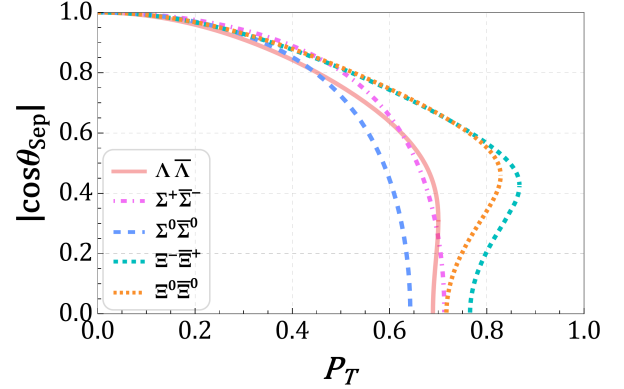


FIG. 13. The $\cos \theta_{Sep}$ as a function of the beam transverse polarization degree P_T in $J/\psi \rightarrow Y\bar{Y}$ for $Y = \Lambda$, Σ^+ , Σ^0 , Ξ^- and Ξ^0 respectively.

Furthermore, under this condition

$$\det \rho_{Y\bar{Y}}^\Gamma = 0, \quad \frac{\partial \det \rho_{Y\bar{Y}}^\Gamma}{\partial \cos \theta} = 0 \quad (40)$$

is satisfied (see Eq. (20)). Then the $\cos \theta_{Sep}$ can be plotted as a function of P_T as shown in Fig. 13 at fixed ϕ^* . For unpolarized lepton beams, the system is separable at $\theta_{Sep} = 0$ and π . It can be seen that increasing the transverse polarization degree moves the θ_{Sep} to the direction of $\pi/2$. There are two θ_{Sep} at some P_T range for $\Lambda\bar{\Lambda}$, $\Sigma^+\bar{\Sigma}^-$ and $\Xi^0\bar{\Xi}^0$ pairs. When the P_T is big enough, the separate state vanishes for all channels.

VI. CONCLUSION

This work systematically investigates the influence of longitudinal and transverse beam polarization on quantum entanglement and Bell nonlocality of hyperon-antihyperon pairs produced in electron-positron annihilation. Based on the explicit spin density matrix, the CHSH parameter, concurrence, and negativity of the $Y\bar{Y}$ system are quantitatively evaluated. It is found that both polarization configurations can enhance quantum correlations, though the manifestation differ remarkably. Longitudinal polarization of beam broadens the angular range of Bell nonlocality and increases monotonically entanglement of the system, but fails to attain maximal entanglement even at maximum polarization degree. In contrast, transverse polarization enables the system to be maximal entangled across full range of scattering angle if choosing optimally the azimuthal angle. The underlying reason is ascribed to different reaction of hyperons polarization to beam polarization modes. Hierarchy of quantum correlations under two polarization configurations of beams and separable state in the case of transversely polarized beams are thoroughly discussed as well.

The decay parameters of $J/\psi \rightarrow \Sigma^+\bar{\Sigma}^+$ and $\Sigma^0\bar{\Sigma}^0$ are negative, opposite to those of $\Lambda\bar{\Lambda}$, $\Xi^-\bar{\Xi}^-$ and $\Xi^0\bar{\Xi}^0$. As a

result, the response of Bell nonlocality and entanglement of $Y\bar{Y}$ system to the manipulation of beam polarization is obviously different. This result as a by product provides another perspective on anomalous decay parameters of $J/\psi \rightarrow \Sigma^+\bar{\Sigma}^+$ and $\Sigma^0\bar{\Sigma}^0$.

Transversely polarized beams would be already available at BESIII as discussed in literature [46], and longitudinally polarized beams would be feasible at future Super τ -Charm facility [81]. The findings in this paper highlight the potential of exploiting polarized beams as a tool to study quantum correlations of $Y\bar{Y}$ system, and also as a means to explore theoretically the quantum information in other high-energy reactions. Whether polarization of beams is helpful for clarifying the scope and limitations of Bell-type reasoning in particle physics is another interesting topic.

ACKNOWLEDGMENTS

This work is supported by the National Key R&D Program of China under Grant No. 2023YFA1606703, the National Natural Science Foundation of China (Grant Nos. 12547111 and 12235008), and the Hebei Natural Science Foundation with Grant Nos. A2022201017 and A2023201041, and Natural Science Foundation of Guangxi Autonomous Region with Grant No. 2022GXNSFDA035068.

Appendix A: Supplementary figures for J/ψ and $\psi(3686) \rightarrow Y\bar{Y}$

TABLE III. The decay parameters of $\psi(3686) \rightarrow Y\bar{Y}$ for $Y = \Lambda, \Sigma^+, \Sigma^0, \Xi^-$ and Ξ^0 .

$\psi(3686) \rightarrow$	α_ψ	$\Delta\Phi/\text{rad}$	Ref
$\Lambda\bar{\Lambda}$	0.690(73)	0.400(143)	[63, 82]
$\Sigma^+\bar{\Sigma}^-$	0.682(32)	0.397(71)	[60, 63]
$\Sigma^0\bar{\Sigma}^0$	0.814(40)	0.512(92)	[61, 63]
$\Xi^-\bar{\Xi}^+$	0.693(69)	0.667(125)	[63, 83]
$\Xi^0\bar{\Xi}^0$	0.665(118)	-0.050(151)	[63, 65]

In Fig. 14 the CHSH parameters and concurrence for $J/\psi \rightarrow \Sigma^0\bar{\Sigma}^0$ are shown as a complementary figures in the main text. In Fig. 15 the negativity of $J/\psi \rightarrow Y\bar{Y}$ for $Y = \Lambda, \Sigma^+, \Sigma^0, \Xi^-$ and Ξ^0 is shown under longitudinal and transverse beam polarization configurations. For the transverse beam polarization, the dashed curve $\mathcal{N}(\theta = 0, \pi) = \mathcal{N}(\theta = \pi/2)$ in lower panels of Fig. 15 divides each panel into two regions. For the region above the dashed curve, the $\max_\theta \mathcal{N}$ locates at $\theta = 0, \pi$. For the region below the dashed curve, the $\max_\theta \mathcal{N}$ locates at $\theta = \pi/2$.

The decay parameters of $\psi(3686) \rightarrow Y\bar{Y}$ for $Y = \Lambda, \Sigma^+, \Sigma^0, \Xi^-$ and Ξ^0 are collected in Table. III. The CHSH

parameter $\mathcal{B}[\rho_{Y\bar{Y}}^{PL}]$, negativity $\mathcal{N}[\rho_{Y\bar{Y}}^{PL}]$ and concurrence $\mathcal{C}[\rho_{Y\bar{Y}}^{PL}]$ are shown in Figs. 16 and 17 for $\psi(3686) \rightarrow Y\bar{Y}$ under longitudinal beam polarization configuration, and those under transverse beam polarization configuration are shown in Figs. 18 and 19. Under the transverse beam polarization, the dashed curve $\mathcal{B}, \mathcal{N}, \mathcal{C}(\theta = 0, \pi) = \mathcal{B}, \mathcal{N}, \mathcal{C}(\theta = \pi/2)$ in Fig. 18 divides each panel into two regions. For the region above the dashed curve, the $\max_\theta \mathcal{B}, \mathcal{N}, \mathcal{C}$ locates at $\theta = 0, \pi$. For the region below the dashed curve, the $\max_\theta \mathcal{B}, \mathcal{N}, \mathcal{C}$ locates at $\theta = \pi/2$.

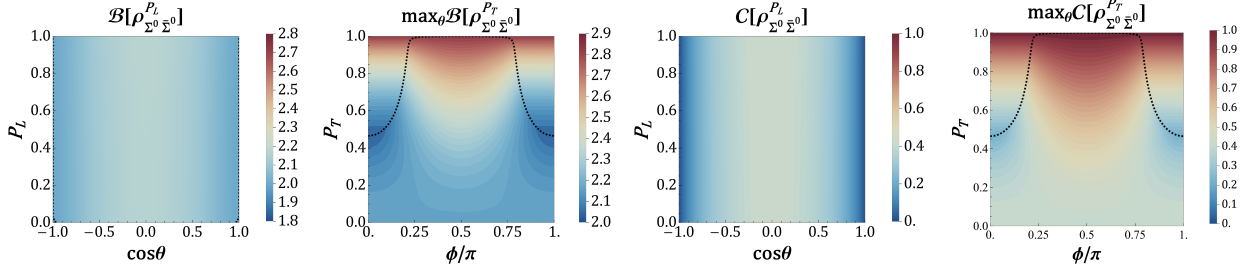


FIG. 14. The CHSH parameters and concurrence for $J/\psi \rightarrow \Sigma^0 \bar{\Sigma}^0$. The dashed curves are for $\mathcal{B}(\theta = 0, \pi) = \mathcal{B}(\theta = \pi/2)$ and $\mathcal{C}(\theta = 0, \pi) = \mathcal{C}(\theta = \pi/2)$, respectively.

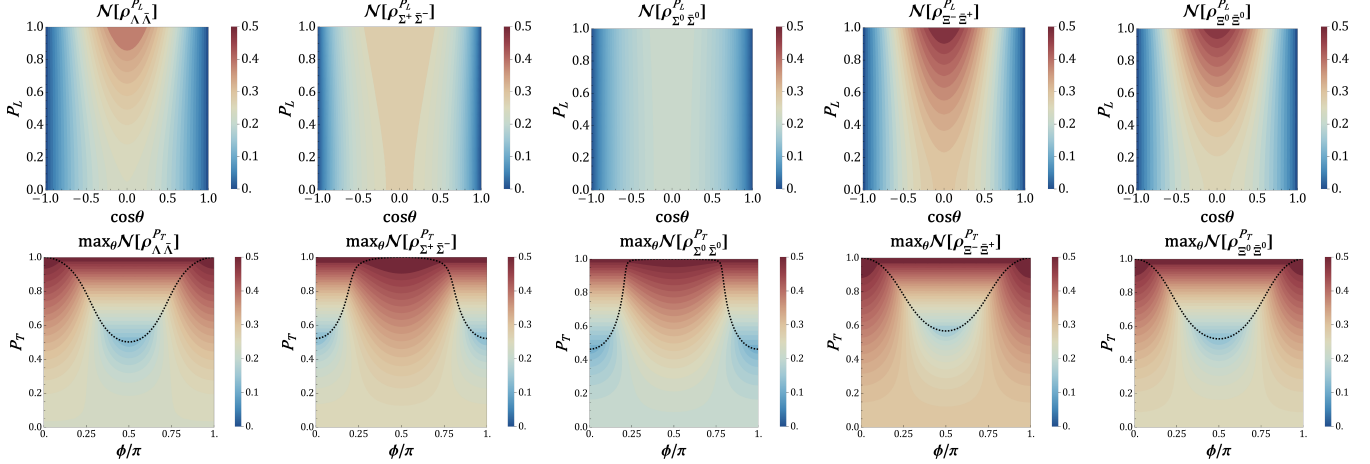


FIG. 15. Negativity $\mathcal{N}[\rho_{Y\bar{Y}}^{P_L}]$ as a function of P_L and θ (upper panels), and the $\max_\theta \mathcal{N}[\rho_{Y\bar{Y}}^{P_T}]$ as a function of P_T and ϕ (lower panels) in $J/\psi \rightarrow Y\bar{Y}$ for $Y = \Lambda, \Sigma^+, \Sigma^0, \Xi^-$ and Ξ^0 . The dashed curve is $\mathcal{N}(\theta = 0, \pi) = \mathcal{N}(\theta = \pi/2)$.

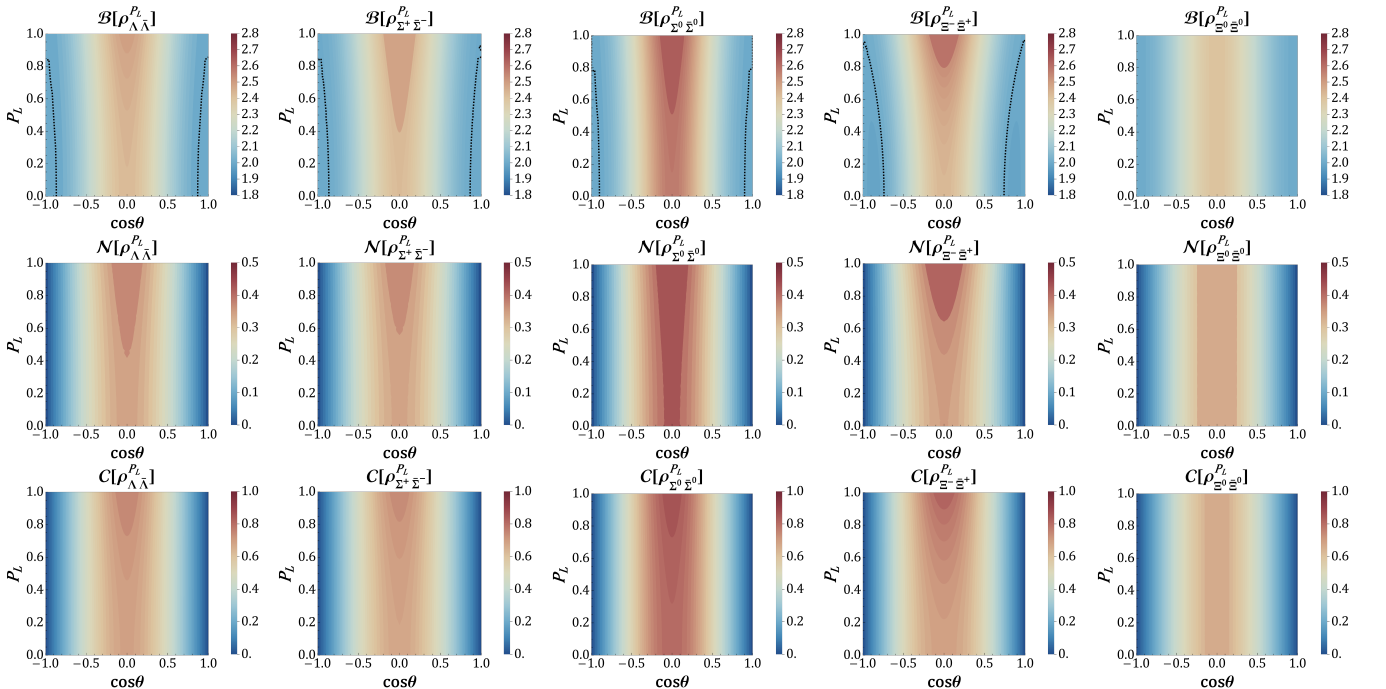


FIG. 16. The CHSH parameter $\mathcal{B}[\rho_{Y\bar{Y}}^{P_L}]$ (upper panels), negativity $\mathcal{N}[\rho_{Y\bar{Y}}^{P_L}]$ (middle panels) and concurrence $\mathcal{C}[\rho_{Y\bar{Y}}^{P_L}]$ (lower panels) as a function of P_L and θ in $\psi(3686) \rightarrow Y\bar{Y}$ for $Y = \Lambda, \Sigma^+, \Sigma^0, \Xi^-$ and Ξ^0 . The dashed line in each of upper panels is $\mathcal{B} = 2$.

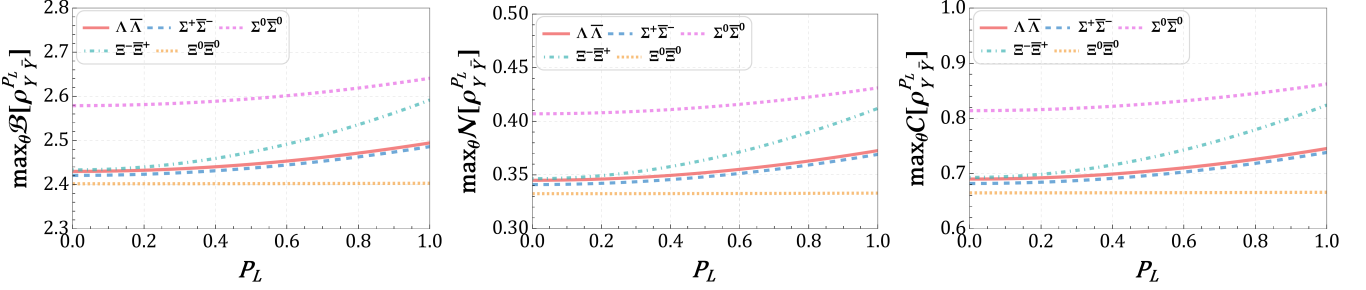


FIG. 17. The $\max_{\theta} \mathcal{B}[\rho_L]$ (left), negativity $\max_{\theta} \mathcal{N}[\rho_L]$ (middle), and concurrence $\max_{\theta} \mathcal{C}[\rho_L]$ (right) as a function P_L and θ in $\psi(3686) \rightarrow Y\bar{Y}$ for $Y = \Lambda, \Sigma^+, \Sigma^0, \Xi^-$ and Ξ^0 .

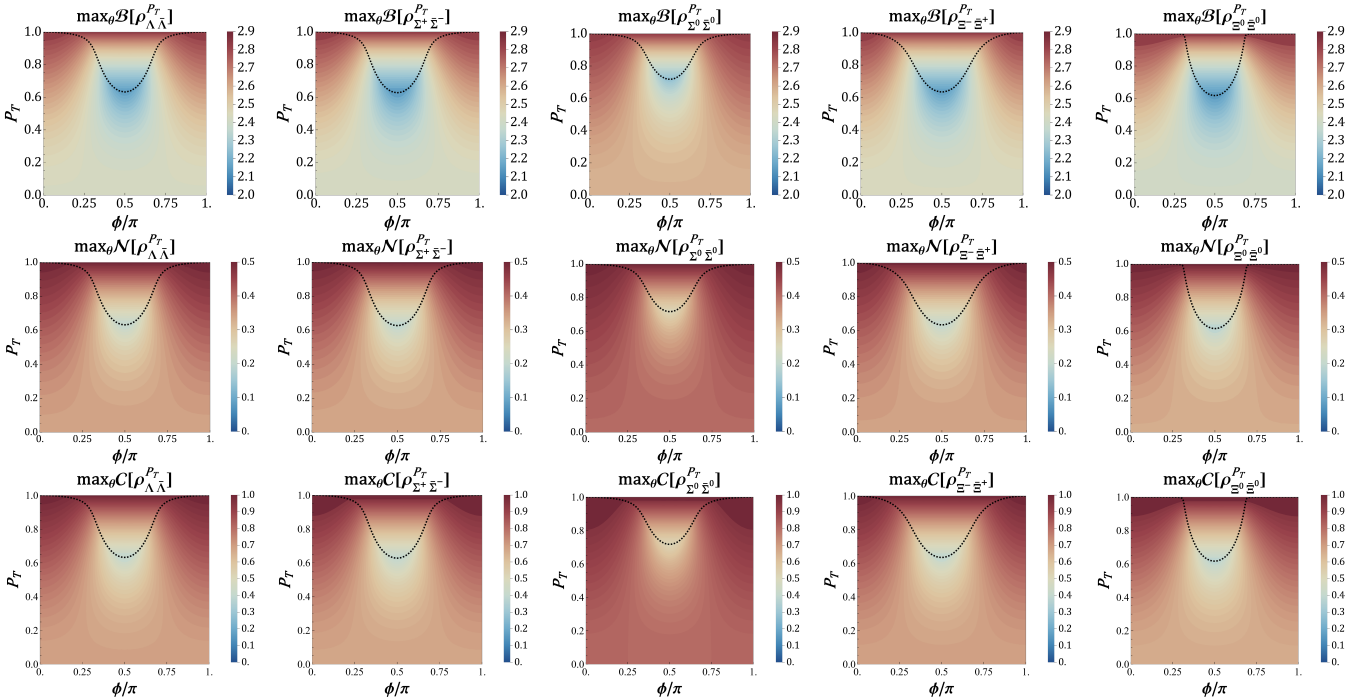


FIG. 18. The $\max_{\theta} \mathcal{C}[\rho_T]$ (upper panels), $\max_{\theta} \mathcal{N}[\rho_T^{P_L}]$ (middle panels), and $\max_{\theta} \mathcal{N}[\rho_T^{P_T}]$ (lower panels) as a function of azimuthal angle ϕ and transverse polarization degree P_T in $\psi(3686) \rightarrow Y\bar{Y}$ for $Y = \Lambda, \Sigma^+, \Sigma^0, \Xi^-$ and Ξ^0 . The dashed curve is $\mathcal{B}, \mathcal{N}, \mathcal{C}(\theta = 0, \pi) = \mathcal{B}, \mathcal{N}, \mathcal{C}(\theta = \pi/2)$ in each of upper, middle and lower panels respectively.

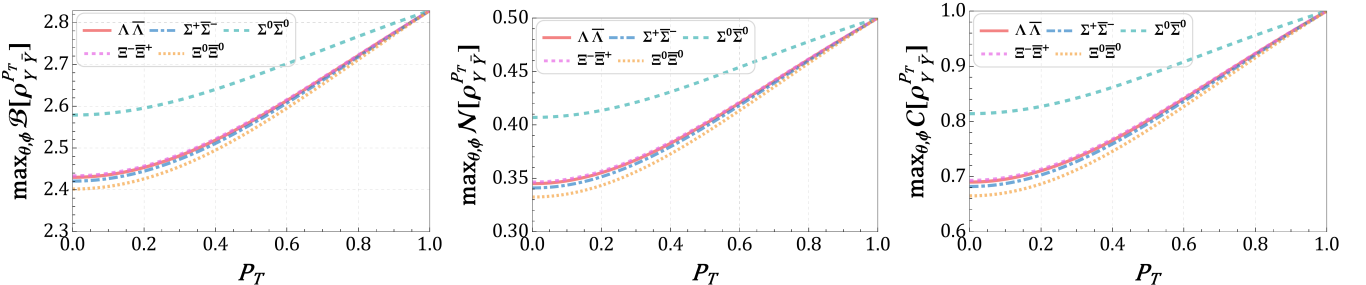


FIG. 19. The $\max_{\theta, \phi} \mathcal{B}[\rho_T]$ (left), $\max_{\theta, \phi} \mathcal{N}[\rho_T]$ (middle), and $\max_{\theta, \phi} \mathcal{C}[\rho_T]$ (right) as a function P_T in $\psi(3686) \rightarrow Y\bar{Y}$ for $Y = \Lambda, \Sigma^+, \Sigma^0, \Xi^-$ and Ξ^0 .

[1] A. Aspect, P. Grangier, and G. Roger, *Phys. Rev. Lett.* **47**, 460 (1981).

[2] H. M. Wiseman, S. J. Jones, and A. C. Doherty, *Phys. Rev. Lett.* **98**, 140402 (2007), arXiv:quant-ph/0612147.

[3] M. Giustina *et al.*, *Phys. Rev. Lett.* **115**, 250401 (2015), arXiv:1511.03190 [quant-ph].

[4] Y. Afik and J. R. M. de Nova, *Eur. Phys. J. Plus* **136**, 907 (2021), arXiv:2003.02280 [quant-ph].

[5] M. Fabbrichesi, R. Floreanini, and G. Panizzo, *Phys. Rev. Lett.* **127**, 161801 (2021), arXiv:2102.11883 [hep-ph].

[6] G. Aad *et al.* (ATLAS), *Nature* **633**, 542 (2024), arXiv:2311.07288 [hep-ex].

[7] A. Hayrapetyan *et al.* (CMS), *Rept. Prog. Phys.* **87**, 117801 (2024), arXiv:2406.03976 [hep-ex].

[8] J. A. Formaggio, D. I. Kaiser, M. M. Murksyj, and T. E. Weiss, *Phys. Rev. Lett.* **117**, 050402 (2016), arXiv:1602.00041 [quant-ph].

[9] M. Fabbrichesi, R. Floreanini, and E. Gabrielli, *Eur. Phys. J. C* **83**, 162 (2023), arXiv:2208.11723 [hep-ph].

[10] M. M. Altakach, P. Lamba, F. Maltoni, and K. Sakurai, (2026), arXiv:2601.09558 [hep-ph].

[11] Y.-C. Guo, T. Han, M. Low, and Y. Su, (2026), arXiv:2602.02719 [hep-ph].

[12] K. Cheng and B. Yan, *Phys. Rev. Lett.* **135**, 011902 (2025), arXiv:2501.03321 [hep-ph].

[13] W. Qi, Z. Guo, and B.-W. Xiao, (2025), arXiv:2506.12889 [hep-ph].

[14] K. Cheng, T. Han, and S. Trifinopoulos, (2025), arXiv:2510.23773 [hep-ph].

[15] Y. Hatta and J. Schoenleber, (2025), arXiv:2511.04537 [hep-ph].

[16] A. Cervera-Lierta, J. I. Latorre, J. Rojo, and L. Rottoli, *SciPost Phys.* **3**, 036 (2017), arXiv:1703.02989 [hep-th].

[17] D. E. Kharzeev and E. M. Levin, *Phys. Rev. D* **95**, 114008 (2017), arXiv:1702.03489 [hep-ph].

[18] Z. Tu, D. E. Kharzeev, and T. Ullrich, *Phys. Rev. Lett.* **124**, 062001 (2020), arXiv:1904.11974 [hep-ph].

[19] M. Hentschinski, D. E. Kharzeev, K. Kutak, and Z. Tu, *Phys. Rev. Lett.* **131**, 241901 (2023), arXiv:2305.03069 [hep-ph].

[20] M. Hentschinski, D. E. Kharzeev, K. Kutak, and Z. Tu, *Rept. Prog. Phys.* **87**, 120501 (2024), arXiv:2408.01259 [hep-ph].

[21] J. Datta, A. Deshpande, D. E. Kharzeev, C. J. Naïm, and Z. Tu, *Phys. Rev. Lett.* **134**, 111902 (2025), arXiv:2410.22331 [hep-ph].

[22] Z. X. Shen, H. Y. Shang, Y. G. Ma, D. Bai, S. M. Wang, and Z. C. Xu, (2025), arXiv:2510.24325 [nucl-th].

[23] S. R. Beane, D. B. Kaplan, N. Klco, and M. J. Savage, *Phys. Rev. Lett.* **122**, 102001 (2019), arXiv:1812.03138 [nucl-th].

[24] Y. Du, X.-G. He, C.-W. Liu, and J.-P. Ma, *Eur. Phys. J. C* **85**, 1255 (2025), arXiv:2409.15418 [hep-ph].

[25] A. Tang, *Phys. Lett. B* **868**, 139820 (2025), arXiv:2507.18507 [nucl-ex].

[26] M. Ablikim *et al.* (BESIII), (2025), arXiv:2506.07907 [hep-ex].

[27] M. Ablikim *et al.* (BESIII), (2025), arXiv:2506.07906 [hep-ex].

[28] N. A. Tornqvist, *Found. Phys.* **11**, 171 (1981).

[29] C. Qian, J.-L. Li, A. S. Khan, and C.-F. Qiao, *Phys. Rev. D* **101**, 116004 (2020), arXiv:2002.04283 [quant-ph].

[30] A. S. Khan, J.-L. Li, and C.-F. Qiao, *Phys. Rev. D* **101**, 096016 (2020), arXiv:2003.04669 [quant-ph].

[31] J. Pei, X. Hao, X. Wang, and T. Li, (2025), arXiv:2505.09931 [hep-ph].

[32] M. Fabbrichesi, R. Floreanini, E. Gabrielli, and L. Marzola, *Phys. Rev. D* **110**, 053008 (2024), arXiv:2406.17772 [hep-ph].

[33] S. Wu, C. Qian, Y.-G. Yang, and Q. Wang, *Chin. Phys. Lett.* **41**, 110301 (2024), arXiv:2402.16574 [hep-ph].

[34] S. Wu, C. Qian, Q. Wang, and X.-R. Zhou, *Phys. Rev. D* **110**, 054012 (2024), arXiv:2406.16298 [hep-ph].

[35] P. Hong, R. Ping, and W. Song, (2025), arXiv:2512.22837 [hep-ph].

[36] E. Jaloum and M. Amazioug, *Phys. Rev. D* **113**, 016024 (2026), arXiv:2510.25615 [quant-ph].

[37] S. Wu, C. Qian, Q. Wang, and Y.-G. Yang, (2025), arXiv:2509.14990 [hep-ph].

[38] M. Ablikim *et al.* (BESIII), *Nature Commun.* **16**, 4948 (2025), arXiv:2505.14988 [hep-ex].

[39] S. A. Abel, M. Dittmar, and H. K. Dreiner, *Phys. Lett. B* **280**, 304 (1992).

[40] H. K. Dreiner, in *2nd Workshop on Tau Lepton Physics* (1992) arXiv:hep-ph/9211203.

[41] S. Li, W. Shen, and J. M. Yang, *Eur. Phys. J. C* **84**, 1195 (2024), arXiv:2401.01162 [hep-th].

[42] M. Low, *Phys. Rev. D* **112**, 096008 (2025), arXiv:2508.10979 [hep-ph].

[43] P. Bechtle, C. Breunig, H. K. Dreiner, and C. Duhr, (2025), arXiv:2507.15947 [hep-ph].

[44] S. A. Abel, H. K. Dreiner, R. Sengupta, and L. Ubaldi, (2025), arXiv:2507.15949 [hep-ph].

[45] T. Ai, Q. Bi, Y. He, J. Liu, and X.-P. Wang, *Phys. Rev. Lett.* **135**, 241804 (2025), arXiv:2506.10673 [hep-ph].

[46] X. Cao, Y.-T. Liang, and R.-G. Ping, *Phys. Rev. D* **110**, 014035 (2024), arXiv:2404.00298 [hep-ph].

[47] U. Fano, *Rev. Mod. Phys.* **55**, 855 (1983).

[48] E. Perotti, G. Fäldt, A. Kupsc, S. Leupold, and J. J. Song, *Phys. Rev. D* **99**, 056008 (2019), arXiv:1809.04038 [hep-ph].

[49] V. Batozskaya, A. Kupsc, N. Salone, and J. Wiechnik, *Phys. Rev. D* **108**, 016011 (2023), arXiv:2302.07665 [hep-ph].

[50] N. Salone, P. Adlarson, V. Batozskaya, A. Kupsc, S. Leupold, and J. Tandean, *Phys. Rev. D* **105**, 116022 (2022), arXiv:2203.03035 [hep-ph].

[51] S. Zeng, Y. Xu, X. R. Zhou, J. J. Qin, and B. Zheng, *Chin. Phys. C* **47**, 113001 (2023), arXiv:2306.15602 [hep-ex].

[52] Z. Zhang, R.-G. Ping, T. Liu, J. J. Song, W. Yang, and Y.-j. Zhou, *Phys. Rev. D* **110**, 034034 (2024), arXiv:2404.04787 [hep-ph].

[53] C.-Q. Zhao, X. Cao, and J.-P. Dai, (2025), arXiv:2512.19085 [hep-ph].

[54] T. Yu and J. H. Eberly, *Quant. Inf. Comput.* **7**, 459 (2007), arXiv:quant-ph/0503089.

[55] W. Dur, G. Vidal, and J. I. Cirac, *Phys. Rev. A* **62**, 062314 (2000), arXiv:quant-ph/0005115.

[56] C. H. Bennett, D. P. DiVincenzo, J. A. Smolin, and W. K. Wootters, *Phys. Rev. A* **54**, 3824 (1996),

arXiv:quant-ph/9604024.

[57] M. Ablikim *et al.* (BESIII), *Nature Phys.* **15**, 631 (2019), arXiv:1808.08917 [hep-ex].

[58] M. Ablikim *et al.* (BESIII), *Phys. Rev. D* **95**, 052003 (2017), arXiv:1701.07191 [hep-ex].

[59] M. Ablikim *et al.* (BES), *Phys. Rev. D* **78**, 092005 (2008), arXiv:0810.1896 [hep-ex].

[60] M. Ablikim *et al.* (BESIII), *Phys. Rev. Lett.* **125**, 052004 (2020), arXiv:2004.07701 [hep-ex].

[61] M. Ablikim *et al.* (BESIII), *Phys. Rev. Lett.* **133**, 101902 (2024), arXiv:2406.06118 [hep-ex].

[62] M. Ablikim *et al.* (BESIII), *Nature* **606**, 64 (2022), arXiv:2105.11155 [hep-ex].

[63] R. L. Workman *et al.* (Particle Data Group), *PTEP* **2022**, 083C01 (2022).

[64] M. Ablikim *et al.* (BESIII), *Phys. Lett. B* **770**, 217 (2017), arXiv:1612.08664 [hep-ex].

[65] M. Ablikim *et al.* (BESIII), *Phys. Rev. D* **108**, L031106 (2023), arXiv:2305.09218 [hep-ex].

[66] J. S. Bell, *Physics Physique Fizika* **1**, 195 (1964).

[67] J. F. Clauser and A. Shimony, *Rept. Prog. Phys.* **41**, 1881 (1978).

[68] J. F. Clauser, M. A. Horne, A. Shimony, and R. A. Holt, *Phys. Rev. Lett.* **23**, 880 (1969).

[69] R. Horodecki, P. Horodecki, and M. Horodecki, *Phys. Lett. A* **200**, 340 (1995).

[70] R. F. Werner, *Phys. Rev. A* **40**, 4277 (1989).

[71] A. Peres, *Phys. Rev. Lett.* **77**, 1413 (1996), arXiv:quant-ph/9604005.

[72] M. Horodecki, P. Horodecki, and R. Horodecki, *Phys. Lett. A* **223**, 1 (1996), arXiv:quant-ph/9605038.

[73] P. B. Slater, *Phys. Rev. A* **71**, 052319 (2005), arXiv:quant-ph/0410238.

[74] R. Augusiak, M. Demianowicz, and P. Horodecki, *Phys. Rev. A* **77**, 030301 (2007), arXiv:quant-ph/0604109.

[75] G. Vidal and R. F. Werner, *Phys. Rev. A* **65**, 032314 (2002), arXiv:quant-ph/0102117.

[76] W. K. Wootters, *Phys. Rev. Lett.* **80**, 2245 (1998), arXiv:quant-ph/9709029.

[77] H. Azuma and M. Ban, *J. Mod. Opt.* **57**, 677 (2010), arXiv:0910.3822 [quant-ph].

[78] A. Sanpera, R. Tarrach, and G. Vidal, *Phys. Rev. A* **58**, 826 (1998), arXiv:quant-ph/9801024.

[79] F. Verstraete and M. M. Wolf, *Phys. Rev. Lett.* **89**, 170401 (2002), arXiv:quant-ph/0112012.

[80] A. J. Barr, M. Fabbrichesi, R. Floreanini, E. Gabrielli, and L. Marzola, *Prog. Part. Nucl. Phys.* **139**, 104134 (2024), arXiv:2402.07972 [hep-ph].

[81] M. Achasov *et al.*, *Front. Phys. (Beijing)* **19**, 14701 (2024), arXiv:2303.15790 [hep-ex].

[82] M. Ablikim *et al.* (BESIII), *JHEP* **10**, 081 (2023), [Erratum: *JHEP* 12, 080 (2023)], arXiv:2303.00271 [hep-ex].

[83] M. Ablikim *et al.* (BESIII), *Phys. Rev. D* **106**, L091101 (2022), arXiv:2206.10900 [hep-ex].